

A HYDRODYNAMIC CRITERION OF ALTERNATIVE BUBBLE DEPARTURES

by

**Pawel DZIENIS^{*}, Romuald MOSDORF, Daniel TOMASZUK,
and Tomasz WYSZKOWSKI**

Bialystok University of Technology, Faculty of Mechanical Engineering,
Bialystok, Poland

Original scientific paper
<https://doi.org/10.2298/TSCI190510417D>

The bubble departures from two neighboring brass nozzles (with inner diameter of 1.1 mm) in three liquids: distilled water, mineral, and synthetic engine oils were investigated. The numerical simulations were used for reconstruction of liquid-flow around the departing bubbles. Bubble movements in liquid have been recorded using a high speed camera. The 2-D bubble paths have been reconstructed using: Laplacian of Gaussian filters, algorithm of detection of local extremes of image brightness and Kalman filter. It was shown that during alternative bubble departures bubble paths become repeatable. The dimensionless number (similar to Strouhal number) was proposed to describe oscillating liquid-flow generated by departing bubbles over the nozzle outlet. Such number was used for defining the hydrodynamic criterion of alternative bubble departures.

Key words: *bubble paths, bubble departures, alternative bubble departure, bubble chains*

Introduction

The study of bubble dynamics is crucial to understand bubble-liquid and bubble-bubble interactions. Bubble-liquid interactions are significant in many technological applications such as bubble column reactors, oil/natural gas transport, boiling heat transfer, etc. Moreover, bubble-liquid interactions are applied in many fields: ocean engineering, chemical engineering or medical science [1, 2].

Alternative bubble departures in water, from neighboring nozzles, were experimentally analysed by Mosdorf and Wyszowski [3]. During this kind of bubble departures the time of bubble growth and the distance between successive bubbles is constant. Departed bubbles form unique structures of bubbles flow above nozzle outlets. The appearance of such structures changes the frequency of bubble departures and their paths, vertical coalescence of bubbles does not appear. During non-alternative bubble departures the distance between successive bubbles changes chaotically. It was shown that the stability of alternative bubble departures is controlled by the distance between nozzles, their arrangement and the air volume flow rate.

The liquid-flow between alternatively departing bubbles can be responsible for stability of alternative bubble departures, therefore in the paper a hydrodynamic aspect of ap-

^{*} Corresponding author, e-mail: p.dzienis@pb.edu.pl

pearance of stable alternative bubble departures was analysed. Bubble movements in liquid have been recorded using a high speed camera. The numerical simulations with using the level-set method (in COMSOL Multiphysics) were used for reconstruction of liquid-flow around the departing bubbles. The dimensionless number (similar to Strouhal number) was proposed to describe oscillating liquid-flow over the nozzle outlet. Such number was used for defining the hydrodynamic criterion of alternative bubble departures. The criterion of appearance of stable alternative bubble departures, proposed in the paper, is a result of analysis of bubble departures from two neighboring brass nozzles and numerical simulations of liquid-flow around the departing bubbles. Experiments were carried out in three types of liquids: distilled water, mineral and synthetic engine oils.

Experimental set-up and signal characteristics

The scheme of experimental set-up is shown in fig. 1. Nozzles – 2 with inner diameter equal to 1.1 mm, were placed in the bottom of a tank (400 × 400 × 700 mm). The tank

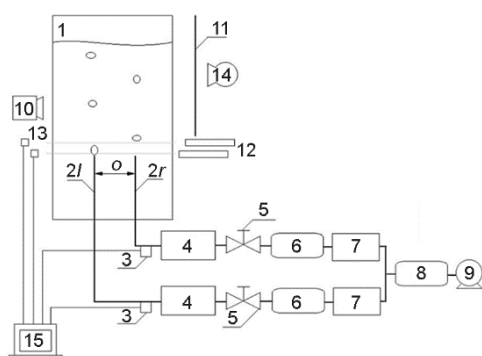


Figure 1. Schema of experimental set-up;
1 – glass tank, 2 – nozzles, 3 – pressure sensors,
4 – flowmeters, 5 – air valves, 6 – air tank,
7 – pressure regulator, 8 – air pump tank,
9 – air pump 10 – light source, 11 – camera,
12 – screen, 13 – lasers, 14 – phototransistors,
15 – computer acquisition system

1 – 1 was filled with: distilled water, synthetic and mineral engine oils. The distance, S , between nozzles was changed from 4 mm to 6 mm in water, and from 4 mm to 10 mm in engine oils. Air was supplied by air pumps – 9) connected to the tank – 8). The proportional pressure reducing valves Metalwork Regtronic – 7) were used to maintain the constant pressure in the tank – 6. The adjustable pressure range of pressure reducing valve was 0.05-10 bar, with accuracy equal to 0.5%. During the experiment the pressure of supplied air was 0.2 bar. The air volume flow rate was measured using the flow meter (MEDSON s.c Sho-Rate-Europe Rev D, P10412A). The accuracy of the flow meter – 4) is equal to 5%. The air volume flow rate was in the range of 0.014 L per minute to 0.125 L per minute. Temperature of liquids was equal to ~ 20 °C and was controlled by the digital thermometer MAXIM DS18B20.

Bubble movement was recorded by a high speed camera – CASIO EX FX 1 – 10. Recorded in grey scale videos (600 fps) have been divided into frames. Using these frames, paths of subsequent departing bubbles were determined. Based on the frames the bubble diameters were evaluated. Diameters of bubble just after departure were equal to ~ 4 mm for distilled water and ~ 6 mm for oils.

The waiting time and bubble growth time was measured using laser – phototransistor sensors – 12, 13. Laser beam was placed about 1 mm above the nozzle outlet. During the bubble growing time, the bubble was passing through the laser beam. Then a voltage on the phototransistor was equal to 5 V. After the bubble departure the laser beam was not obscured. The value of voltage was equal to 0.1 V. Time series of voltage changes were recorded using data acquisition station (DT9800 – 15) with sampling frequency of 1 kHz. Time series were used to estimate: bubble departures frequency and the correlation coefficient of bubble departures from neighboring nozzles.

Bubble paths in alternative bubble departures

The path of the bubble departed from single nozzle depends on bubble diameter [4, 5]. The shapes of bubble paths are associated with bubble Reynolds number. In the case, when the Reynolds number is lower than 600, then the shapes of paths are rectilinear. When the Reynolds number is greater than 600, the shape of bubble path becomes zigzag, helical or chaotic [6]. When bubbles are generated from two neighboring nozzles, then the shape of bubble paths depend on the liquid velocity which is modified by neighboring bubbles. Moreover shapes of bubble paths depend on the forces acting on bubbles. Such forces are generated by liquid-flows induced by moving bubbles. Bubble paths repeatability depends on the stability of such liquid-flows. Mougin and Magnaudet [7] show that wake instability and anisotropic added – mass effects are responsible for bubble path instability. Moving bubble leaves the two tubes of stream-wise liquid vorticity, such liquid vorticity is responsible for the appearance of lift force acting on the bubbles [8]. Chaotic bubble movement is generated by the liquid-flow behind the bubble when liquid-flow becomes unstable and the vortical structures become asymmetric [9]. In Augustyniak *et al.* [10] the stability of bubble paths (departed from single nozzle) was investigated. It was shown that the small distribution of the initial conditions of bubble departure influences on the process of appearance of chaotic bubble paths inside the bubble chain. It can be assumed that, the analysis of repeatability of bubbles paths and their shapes can inform us about stability of liquid-flow around the bubbles.

There are a lot of methods of bubble paths reconstructions presented in [11, 12]. In the present paper, the bubble paths have been reconstructed using: a Laplacian of Gaussian filter (LoG) [13, 14], algorithm of detection of local extremes of image brightness and Kalman filter [15, 16] with Hungarian algorithm [17]. The each frame of video was filtered by the LoG filter. In such a way the monochromatic frames, where local extremes of image brightness were treated as the centres of bubbles, were produced. The extrema detection algorithm was used for estimation of the bubble locations. Bubble positions obtained in such a way were treated as the input for the Kalman filter which was used to predict the new positions of bubbles. These positions were compared (using Hungarian Algorithm) with positions obtained using the LoG filter from the next frame. The aforementioned algorithm was used for the next frames. Example of 2-D bubble paths reconstruction is shown in fig. 2 where one hundred paths of subsequent departing bubbles have been presented. The measurement errors significantly depend on the image resolution (in the experiment the image resolution was 432×192 pixels). The maximum measurement error was equal to ± 0.17 mm. Just after bubble departures the bubble paths are repeatable, therefore in fig. 2 the single paths are not visible (the distances between bubble paths are very small). The variation of bubbles lateral displacements increases together with increase in the distance above the outlets of nozzles, therefore in this case single bubble paths become visible (in this case bubble paths are

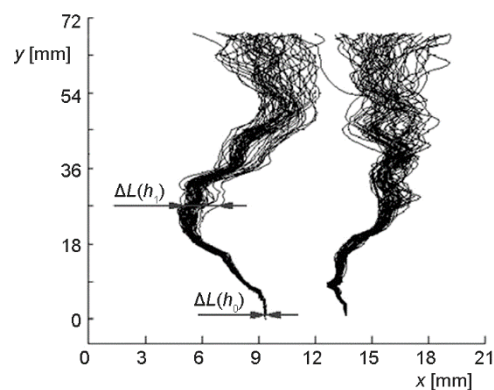


Figure 2. Example of reconstructed paths of departure bubbles for air volume flow rate $q = 0.0645$ L per minute and distance between nozzles $S = 4.5$ mm

unrepeatable). Bubble paths were reconstructed for subsequent departed bubbles. Interactions between flows generated by neighboring bubbles were responsible for appearance of the asymmetrical bubble paths above the neighboring nozzles.

The repeatability of bubble paths was measured using λ_h exponent calculated (for one hundred paths) according to:

$$\lambda_h(q, S) = \log_2 \left[\frac{\Delta L(q, S, h_1)}{\Delta L(q, S, h_0)} \right] \quad (1)$$

where $\Delta L(h_1) = L_{\text{right}} - L_{\text{left}}$ is the distance between the most right and left path on the height of first bubble paths bend and $\Delta L(h_0)$ is the distance between the most right and left path on the height of bubble departure.

The coefficient λ_h is a measure of changing the distance $\Delta L(h_0)$ between the most left and right path. Such distances have been shown in fig. 2 for the left nozzle. The value of $\Delta L(h)$ strongly depends on the height above the nozzle outlet. Heights of h_0 and h_1 were estimated for presented experimental data. The $h_0 = 3$ mm is the beginning location of the bubble just after bubble departure and $h_1 = 27$ mm is the height of first bubble paths bend. For h_1 the distance between bubbles departed from neighboring nozzles becomes the largest in alternative bubble departures. When the bubble paths are repeatable, then the value of λ_h is close to zero.

The occurrence of alternative bubble departures was measured by the following correlation coefficient [3]:

$$C_{0.3s} = \frac{\text{Cov}(x_{i,L}, x_{i,R})}{\sigma_{x,L} \sigma_{x,R}} \quad (2)$$

where Cov is the covariance, σ – the standard deviation, $x_{i,L}$, $x_{i,R}$ are time series recorded by laser phototransistor sensors for the left and right nozzle.

The appearance of alternative bubble departures has been estimated using the average value of the correlation coefficient $C_{0.3s}$ in the moving window of length of 0.3 seconds. Values of the coefficient $C_{0.3s}$, presented in fig. 3, are average values from the calculated time series. When $|C_{0.3s}|$ is close to 1, time series $x_{i,L}$, $x_{i,R}$ are correlated, but when $|C_{0.3s}|$ is close to zero, the time series $x_{i,L}$, $x_{i,R}$ are not correlated. When value of $C_{0.3s}$ is greater than 0, then bubbles depart (from twin nozzle) in the same time. When value of $C_{0.3s}$ is lower than 0, then bubbles depart alternatively.

Bubble paths in water

Bubble paths for selected air volume flow rates and distance between nozzles are shown in fig. 3.

When the air volume flow rate was equal to 0.0530 L per minute, fig. 3(a), $q = 0.0645$ L per minute, fig. 3(b) and distance between nozzles $S = 4$ mm, the bubble paths were repeatable. Repeatability of bubble paths occurs up to the height of 27 mm above nozzle outlet. The increase of air volume flow rate causes the disappearance of alternative bubble departures and bubble paths repeatability, fig. 3(b). Moreover, the increase of the distance between nozzles causes the disappearance of alternative bubble departures and bubble paths repeatability, fig. 3(d).

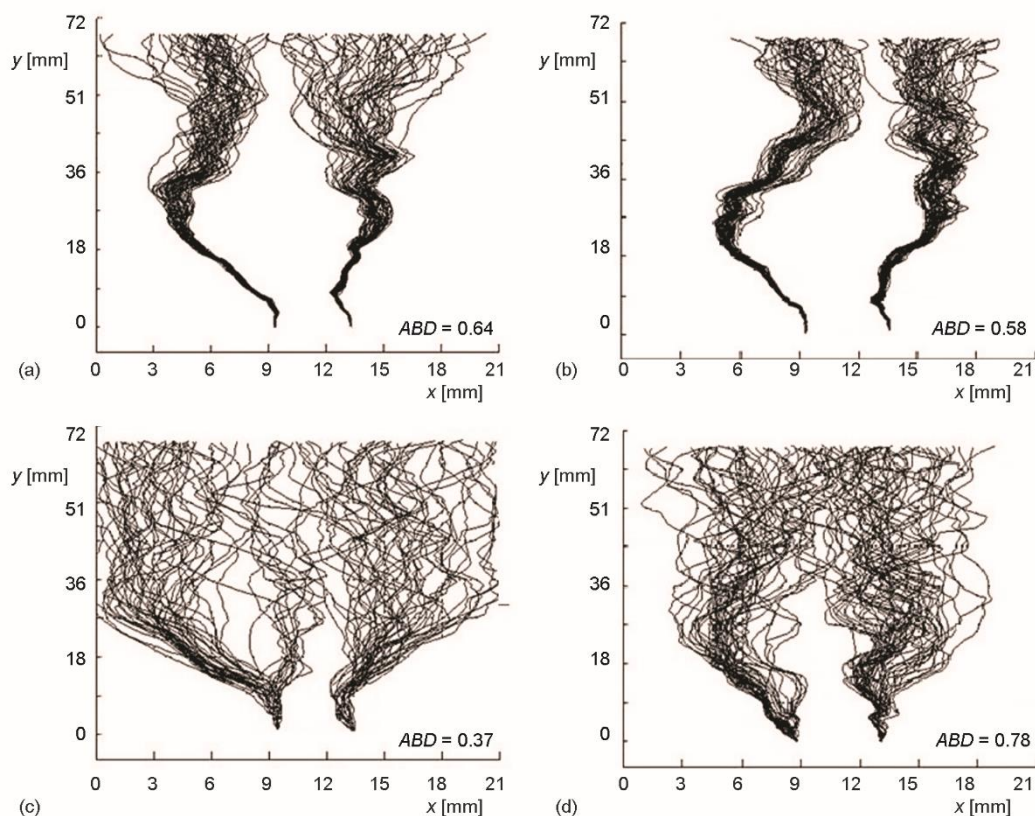


Figure 3. Paths of departing bubbles for selected air volume flow rates, q , and distances between nozzles; (a) $q = 0.0530$ L per minute, $S = 4$ mm – $C_{0.3s} = -0.41$, (b) $q = 0.125$ L per minute, $S = 4$ mm – $C_{0.3s} = -0.08$, (c) $q = 0.0645$ L per minute, $S = 4$ mm – $C_{0.3s} = -0.39$, (d) $q = 0.0645$ L per minute, $S = 4.5$ mm – $C_{0.3s} = -0.04$

In figs. 4(a) and 4(b) values of exponent λ_h for different distances between the nozzles and different air volume flow rates are shown. The values of exponent λ_h were calculated for both nozzles separately. We can notice that repeatability of bubble paths over both nozzles is similar. The exponent λ_h reaches the low value for q in a range 0.053 to 0.0907 L per minute. In this range its value does not change significantly. Minimum value of exponent λ_h indicates the parameters ($q = 0.053$ L per minute, $S = 4$ mm), for which the bubble paths are the most repeatable.

In fig. 4(c) the changes of λ_h exponent vs. the height above the nozzle outlet are shown. The height above the nozzle outlet was calculated in the range from 4 mm to 68 mm. The obtained results show that interactions between bubbles during the alternative bubble departures cause repeatability of bubble paths, when the distance from nozzle outlet is lower than 27 mm. Repeatable paths start to be unrepeatable when the distance between bubbles becomes the largest, in this case it is 27 mm over the nozzle outlet. Disappearance of alternative bubble departures causes that bubble paths become unrepeatable, fig. 4(c), in all distances above nozzle outlets.

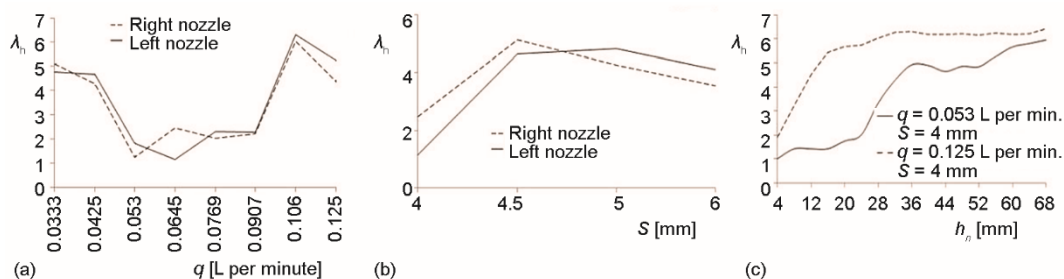


Figure 4. Repeatability of bubble paths vs. air volume flow rates and distance between nozzles; (a) values of exponent λ_h vs. air volume flow rates with constant distance between the nozzle equal to 4 mm, (b) values of exponent λ_h vs. distance between the nozzles with constant $q = 0.0645$ L per minute, (c) changes of λ_h exponent vs. the height above the nozzle outlet for $q = 0.053$ L per minute and $S = 4$ mm (alternative bubble departures) and $q = 0.125$ L per minute, and $S = 4$ mm (non-alternative bubble departures)

Bubble paths in oils

Bubble paths in engine oils were reconstructed only for distance between nozzles equal to 10 mm, because the low oil transparency makes impossible the identification of bubble position for distances between nozzles less than 10 mm. Typical bubble arrangements in the bubble chains and bubble paths in the mineral oil have been shown in fig. 5(a). Typical paths of bubbles and bubble arrangements in the bubble chains in synthetic oil were presented in fig. 5(b).

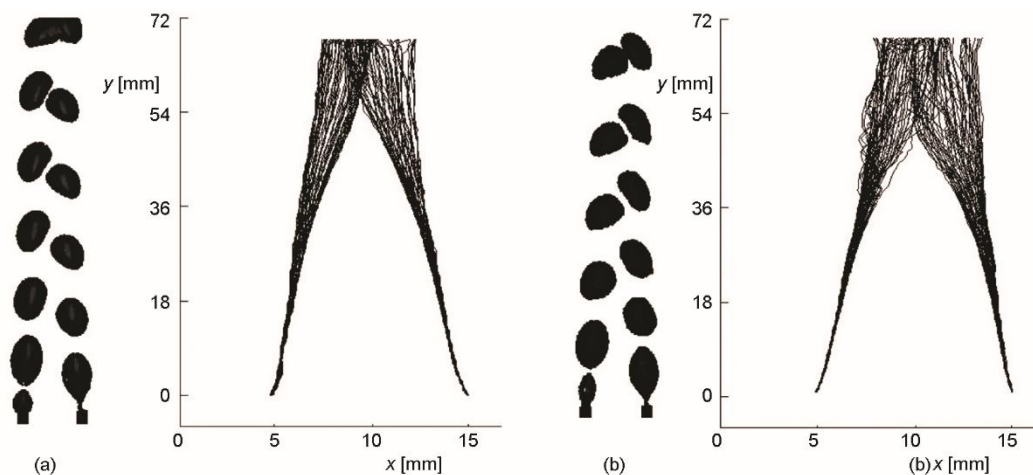


Figure 5. Bubble arrangement in bubble chain and bubble paths for distance between nozzles $S = 10$ mm and air volume flow rate $q = 0.125$ L per minute; (a) mineral oil for $C_{0.3s} = -0.06$, (b) synthetic oil $C_{0.3s} = -0.02$; kinematic viscosity of mineral oil is equal to $53 \text{ mm}^2/\text{s}$ and its density is equal to $850 \text{ kg}/\text{m}^3$

Physical properties of mineral and synthetic engine oils basing on the safety data sheet for oils: kinematic viscosity of mineral oil is equal to $107 \text{ mm}^2/\text{s}$ and its density is equal to $850 \text{ kg}/\text{m}^3$, kinematic viscosity of mineral oil is equal to $53 \text{ mm}^2/\text{s}$ and its density is equal to $850 \text{ kg}/\text{m}^3$ (for liquid temperature $20 \text{ }^\circ\text{C}$).

Liquid-flow around the bubbles

The model of liquid-flow around the bubbles was prepared in COMSOL Multiphysics with the use of CFD Module. The Navier-Stokes eqs. (3) and (4) in 2-D area were solved. The values of κ , n and δ are determined by eqs. (5)-(7) [18]. The density and dynamic viscosity are defined by level set function. The level set function identify the presents of liquid and gas in the 2-D area. The level set function is a continuous function [18]. The interface between the liquid and gas is treated as a contour, where the function $\phi = 0.5$. Regions where $\phi < 0.5$ represent the liquid and region where $\phi > 0.5$ represent the air. The level set function is used to define the density, ρ , and the dynamic viscosity, μ , in two phase flow described by eqs. (9) and (10). The time evolution of level-set function is described by eq. (11) [18].

$$\nabla u = 0 \quad (3)$$

$$\rho \frac{\partial u}{\partial t} + \rho(u \nabla)u = \nabla \left[-pI + \mu(\nabla u + \nabla u^T) \right] + F + \rho g + \sigma \kappa \delta n \quad (4)$$

where u is the velocity, g – the gravity, t – the time, I – the identity matrix, p – the pressure. Expression $\sigma \kappa \delta n$ donates surface tension forces at the interface where δ is the surface tension coefficient, κ – the curvature, n – the unit normal to the interface, δ – the Dirac delta function concentrated to the interface, and F – the speed function:

$$n = \frac{\nabla \phi}{|\nabla \phi|} \quad (5)$$

$$\kappa = \nabla \left(\frac{\nabla \phi}{|\nabla \phi|} \right) \quad (6)$$

$$\delta = 6|\nabla \phi| |\phi(1+\phi)| \quad (7)$$

$$\rho = \rho_l + (\rho_a - \rho_l)\phi \quad (9)$$

$$\mu = \mu_l + (\mu_a - \mu_l)\phi \quad (10)$$

where ρ_l is the liquid density, ρ_a – the air density, μ_l – the dynamic viscosity of liquid, μ_a – the dynamic viscosity of air.

$$\frac{\partial \phi}{\partial t} + u \nabla \phi = \gamma \nabla \left(\varepsilon \nabla \phi - \phi(1-\phi) \frac{\nabla \phi}{|\nabla \phi|} \right) \quad (11)$$

The parameter ε determines the thickness of the region where the function ϕ passes from 0 to 1 and is treated as the size of the elements of the mesh. The parameter γ establishes the reinitialization or stabilization numbers of the level set function [19].

The level set method was unstable in the long period of time, therefore the structure of liquid-flow after the 0.1 seconds of bubble movement was considered in the paper. The initial positions of bubbles are shown in fig. 6(d). In figs. 6(a)-6(c) liquid-flow around four bubbles (after the 0.1 seconds) is shown. The bubble diameter was equal to 4.6 mm. The present model, in comparison with the model presented by Mosdorf and Wyszowski [3] allowed us to analyse the liquid-flow around the single bubbles in bubble column.

The liquid-flow shown in fig. 6(a) was treated as a reference situation. In numerical simulations the physical properties of water (with the temperature equal to 20 °C) were as

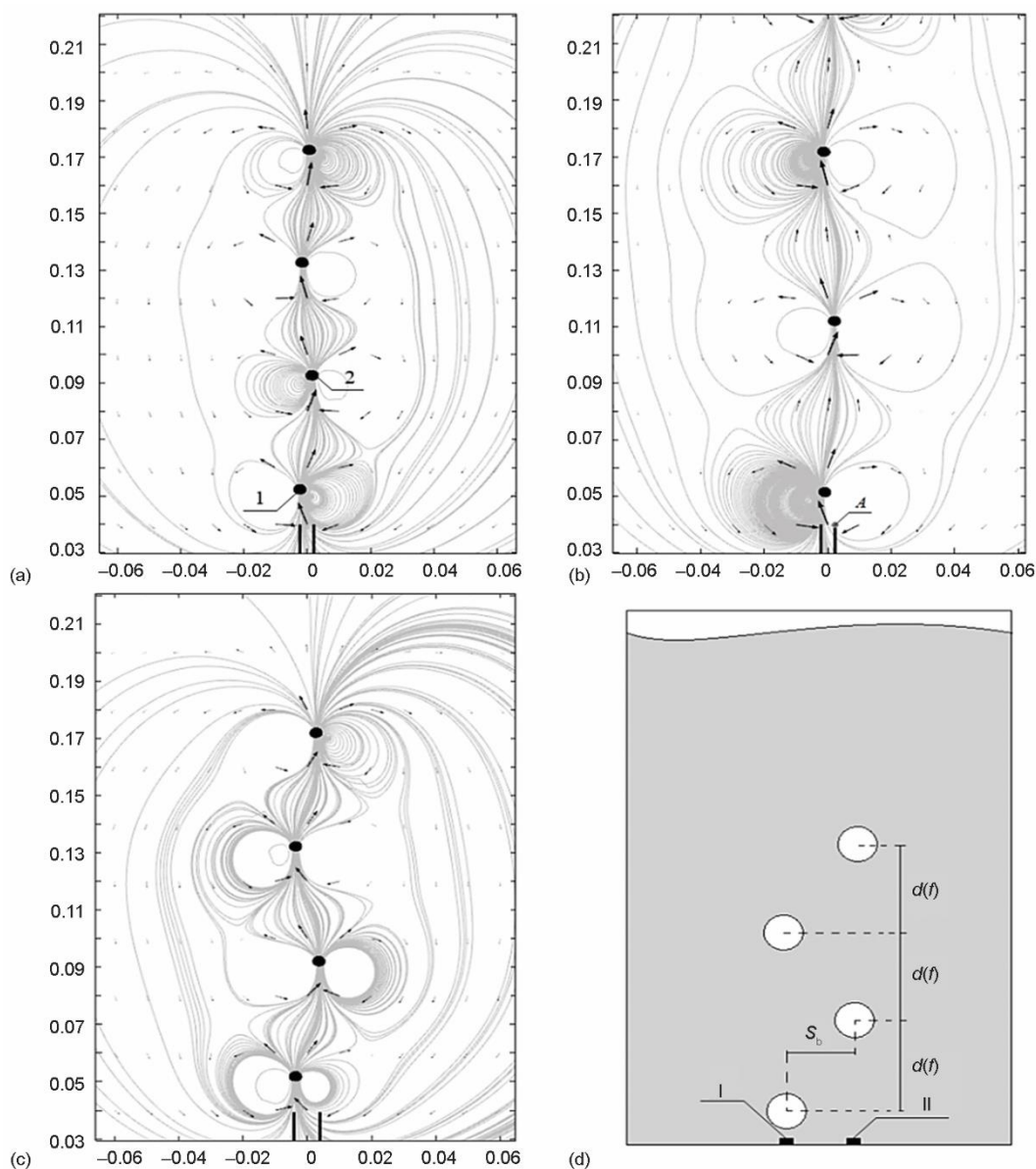


Figure 6. Structures of the liquid-flow around the four bubbles forming the bubble chains over the neighboring nozzles, the pictures present the liquid-flow after the 0.1 seconds of bubbles movement; (a) $S_b = 4$ mm and $d(f) = 4$ mm, (b) $S_b = 6$ mm and $d(f) = 4$ mm, (c) $S_b = 4$ mm, and $d(f) = 8$ mm, (d) schema of initial position of bubbles

follows: density – 998.23 kg/m³, kinematic viscosity – 1.0068 mm²/s and surface tension force – 0.072 N/m. It was analysed the changes of liquid-flow over the nozzle II outlet occurring due to vertical and horizontal changes of initial distance between bubbles. The initial vertical distance between bubbles is related with the frequency of bubble departures. The liquid-flow when the initial vertical distance between the bubbles, $d(f)$, is greater than in case shown

in fig. 6(a) is shown in fig. 6(b). The liquid-flow, where the horizontal distance between nozzles, S_b , is greater than in case shown in fig. 6(a), is shown in fig. 6(c).

In fig. 6(a) the stream lines of liquid-flow around bubbles for the initial distance between the nozzles equal to 4 mm and the initial vertical distance between bubbles equal to 40 mm are shown. At the right side of the bubble 1 the liquid circulation with a high velocity gradient is formed. That liquid circulation strongly affects the formation of bubble at the neighboring nozzle II. We can assume that such liquid circulation is responsible for the synchronization of bubble departures – the creation of alternative bubble departures and repeatability of bubble paths.

In order to evaluate the influence of vertical and horizontal initial distances between bubbles on the hydrodynamic conditions above the nozzle II, the value of vertical liquid velocity above the nozzle II outlet was calculated at the point A – marked in fig. 6(b). The vertical liquid velocity above the nozzle II outlet (after the 0.1 seconds) *vs.* horizontal and vertical distances between bubbles are shown in fig. 7.

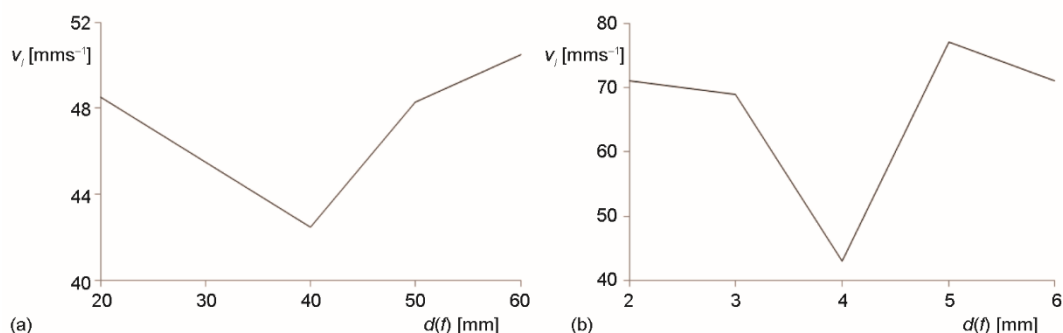


Figure 7. Changes of vertical liquid velocity above the nozzle outlet *vs.* changes of distance between bubbles; (a) changes of vertical distance between bubbles (changes of bubble departure frequency), and (b) changes of horizontal distance between bubbles (changes of distance between nozzles)

We can conclude that the intensity of liquid circulation on the right side of the bubble 1 depends on the distance between nozzles and the frequency of bubble departures. Such liquid circulation enables the bubble 1 the influence on the bubble, which rises over the neighboring nozzle II. The results of simulations presented in fig. 7 show that the appropriate selection of the distance between nozzles and the frequency of bubble departures minimizes the liquid vertical velocity above the nozzle II. In such a way this liquid circulation creates the hydrodynamic mechanism of synchronization of bubble departures.

Dimensionless criterion of alternative bubble departures

The criteria of bouncing bubbles and bubble coalescence have been discussed in the paper [20], where Morton, Reynolds, and Weber numbers have been analysed. It has been found that in case when bubbles are generated in water and the Reynolds number is greater than 600, and the Morton number is of the order of 1×10^{-11} , then the departed bubbles begin to bounce. When the value of Reynolds number increases or the value of the Morton number decreases then the departed bubbles start to coalesce. Such criterion was not fulfilled in silicon oils. The main aim of the present studies was establishing a criterion of occurrence of alternative bubble departures in different kinds of liquids.

The dimensionless numbers were estimated for 50 different cases. The air volume flow rate, distance between nozzles and kind of liquids were changed. In tab. 1 the values of Reynolds, Morton, Bond, and Weber numbers for only characteristic cases – alternative and non-alternative bubble departures in water and engine oils were shown.

Table 1. Values of Reynolds, Morton, Bond, and Webber numbers for selected air volume flow rates, distance between nozzles $S = 4$ mm

Liquid	q [L per minute]	Way of bubble departure	Re	Mo	Bo	We	ABD
Water	0.0333	non-alternative	1242.54	$3 \cdot 10^{-11}$	2.36	5.20	0.84
Water	0.0530	alternative	860.83	$3 \cdot 10^{-11}$	2.62	2.47	0.64
Water	0.0645	alternative	860.83	$3 \cdot 10^{-11}$	2.55	2.40	0.58
Mineral oil	0.0645	non-alternative	11.83	$2.4 \cdot 10^{-2}$	10.45	6.72	0.66
Mineral oil	0.0769	alternative	5.61	$2.4 \cdot 10^{-2}$	9.38	1.59	0.50
Mineral oil	0.1250	non-alternative	17.28	$2.4 \cdot 10^{-2}$	9.91	14.74	0.36
Synthetic oil	0.0645	non-alternative	18.23	$1.6 \cdot 10^{-3}$	6.23	5.25	0.48
Synthetic oil	0.0769	non-alternative	9.12	$1.6 \cdot 10^{-3}$	6.23	1.31	0.42
Synthetic oil	0.1250	non-alternative	24.37	$1.6 \cdot 10^{-3}$	7.11	8.78	0.32

During the alternative bubble departures the values of Reynold and Webber numbers decrease. It is caused by decrease of vertical liquid velocity above the nozzle outlet, which causes the decreases of bubble departure velocity, v_b . Numerical simulations presented in fig. 7 confirm this assumption. Numerical simulations show, that the departing bubble forms a liquid circulation above the neighboring nozzle outlet. Such liquid circulation occurs after each bubble departure. Numerical simulations also show that intensity of such liquid circulation depends on the frequency of bubble departure and the distance between nozzles. The liquid circulation influences on the bubble growth at the neighboring nozzle. Therefore, the synchronisation force should depend on the velocity of growing bubble. Such velocity depends on the air volume flow rate and the nozzle diameter. Finally we can conclude that the dimensionless number describing the synchronization force should be a function of: bubble departures frequency, distance between nozzles and the velocity of bubble growth.

The velocity of the bubble growth was estimated as:

$$v_b \approx \frac{q_b}{r_b^2} \quad (3)$$

where r_b is the radius of growing bubble and q_b – the air volume flow rate supplied to bubble.

The following dimensionless number describing the alternative bubble departure was defined:

$$ABD = \frac{f_b S}{v_b} = \frac{f_b S r_b^2}{q_b} \quad (12)$$

Such formula is similar to the Strouhal number, which is defined as follows [21]:

$$St = \frac{fA}{v} \quad (13)$$

where v is the free stream velocity, f – the frequency of vortex shedding, and A – the amplitude of oscillations.

Subsequent departed bubbles form around the nozzle outlets the liquid circulations which change in time. These liquid circulations affect the initial conditions of bubble movement and finally the shape of their paths. The repeatability of subsequent bubble paths observed in experimental investigations suggests that changes in time of liquid circulations near the nozzle outlets are periodic.

The obtained results are in accordance with the results presented in [3], where it is shown that the alternative bubble departure prevents their chaotic departures. Moreover, the results of the analyses presented by Dzienis and Mosdorf [22] and Mosdorf *et al.* [23] show that the periodicity of changes in the liquid-flow above the nozzle outlet is accompanied by periodic changes in pressure in air supply system. Thus, the alternative bubble departures are related to the synchronization of liquid-flow generated by the moving bubbles as well as the pressure changes in air gas supply system.

The analysis of collected data for water and two engine oils shows, that the alternative bubble departures occur when $0.5 < ABD < 0.64$.

Conclusions

In the paper the bubble departures from two neighboring brass nozzles (with inner diameter of 1.1 mm) in distilled water, mineral and synthetic engine oils were investigated. The original method of bubble paths reconstruction and measurement of its repeatability was proposed. The 2-D bubble paths have been reconstructed using: Laplacian of Gaussian filters, algorithm of detection of local extremes of image brightness and Kalman filter. It has been shown that:

- repeatability of paths of bubbles depends on the air volume flow rates and distance between nozzles,
- alternative bubble departures increase the length of repeatable bubble paths,
- during alternative bubble departures:
 - lengths of repeatable bubble paths are limited, and
 - lengths of repeatable bubble paths are the same over each nozzle.

A hydrodynamic criterion of appearance of alternative bubble departures has been proposed. The criterion was established using the dimensionless number. It has been found that alternative bubble departures occur when the value of dimensionless number ADB is in the range $0.5 < ABD < 0.64$.

The obtained criterion of appearance of alternative bubble departures is in the form of range of values of ADB number. This suggests that the necessary condition of appearance of the alternative departures is connected with the appropriate selection of the distance between the nozzles and the frequency of bubble departures. Those appropriate values of distance between nozzles and appropriate frequency of bubble departures cause that liquid circulation around the departing bubble influences on the bubble growing over the neighboring nozzle.

Acknowledgment

The study has been accomplished under the research project UMO-2011/03/N/ST8/04079 financed by the Polish National Science Centre.

- [15] Kalman, R. E., A New Approach to Linear Filtering and Prediction Problems, *J. Basic Eng.*, 82 (1960), 1, pp. 35-45
- [16] Negenborn, R., Robot Localization and Kalman Filters, On Finding Your Position in a Noisy World, M. Sc. thesis, Institute of Information and Computing Sciences, Utrecht, The Netherland, 2003
- [17] Kuhn, H. W., The Hungarian Method for the Assignment Problem, *Naval Research Logistics Quarterly*, 2 (1955), 1-2, pp. 83-87
- [18] Osher, S., Sethian, J. A., Fronts Propagating with Curvature-Dependent Speed: Algorithms Based on Hamilton-Jacobi Formulations. *J. Comp. Phys.*, 79 (1988), 1, pp. 12-49
- [19] Kass, M., *et al.*, Snakes – Active Contour Models., *Int. J. Comp. Vis.*, 1 (1987), 4, pp. 321-331
- [20] Sanada, T., *et al.*, Motion and Coalescence of a Pair of Bubbles Rising Side by Side, *Chem. Eng. Sci.*, 64 (2009), 11, 2659-2671
- [21] Sakamoto, H., Haniu, H., A Study on Wortex Shedding from Spheres in a Uniform Flow, *J. Fluids Eng.*, 112 (1990), 4, pp. 386-392
- [22] Dzienia, P., Mosdorf, R., Stability of Periodic Bubble Departures at a Low Frequency, *Chem. Eng. Sci.*, 109 (2014), Apr., pp. 171-182
- [23] Mosdorf, R., *et al.*, The Loss of Synchronization between Air Pressure Fluctuations and Liquid Flow Inside the Nozzle During the Chaotic Bubble Departures, *Meccanica*, 52 (2017), 11-12, pp. 2641-2654